Editors' Suggestion

Generation of charge current by the inverse Stern-Gerlach effect in semiconductors

N. J. Harmon,* E. Z. Kurth, D. Coleman, and L. Flanigan
Department of Physics and Engineering Science, Coastal Carolina University, Conway, South Carolina 29526, USA

(Received 27 June 2023; revised 30 April 2024; accepted 1 May 2024; published 15 May 2024)

The spin-orbit interaction is popular for spintronic applications since, through the mechanism of spin-dependent asymmetric scattering, spin currents are generated from charge currents (spin Hall effect) or charge currents are generated from spin currents (inverse spin Hall effect). The discovery of spin, a century ago, relied on a magnetic field gradient to separate opposite spins; this mechanism has received scant attention as a means for generating spin and charge currents in semiconductors. Through the derivation of a set of coupled spin-charge drift-diffusion equations, our paper shows that magnetic field gradients can be used to generate charge currents from nonequilibrium spin polarization in confined solid state systems. We predict, in GaAs, a longitudinal "Stern-Gerlach" voltage. Nonintuitively, we find the spin diffusion length is reduced by the magnetic gradient, which has ramifications for interpreting spin transport experiments. This suppression is understood by invoking the idea of cocurrent and countercurrent exchange, which is a concept found in fields as disparate as animal physiology and thermal engineering.

DOI: 10.1103/PhysRevB.109.195423

I. INTRODUCTION

In 1922, Stern and Gerlach discovered quantized spin angular momentum in neutral silver atoms when an inhomogeneous magnetic field spatially separated discrete spin states [1–3]. The Stern-Gerlach experiment's detection of spin was indirect as it measured the spin of a neutral atom and not the spin of a free charge. Debate arose in the early days of quantum theory whether the spin of a free electron could be verified with a Stern-Gerlach experiment [4–6]. The conventional wisdom that emerged (despite [7,8]), repeating the arguments of Bohr and Mott (see [9–11]), is that Lorentz forces obscure any magnetic moment deflections; since $\nabla \cdot \boldsymbol{B} = 0$, the Lorentz force cannot be avoided by directing motion of spin carriers parallel to $\boldsymbol{B}$ since a gradient field force transverse to the motion also exists. What is overlooked, aside from a few authors [12–14], is these arguments apply for *free* electrons, which is not the condition in which electrons exist in solid state systems. In a confined geometry, the Lorentz force, which is the primary obstacle to spin separation, and the transverse gradient force (due to $\nabla \cdot \boldsymbol{B} = 0$) would be negated by the classical Hall effect. Fabian and Das Sarma studied the effect of inhomogeneous fields on one-dimensional conduction spin currents by solving the Boltzmann equation for a limited set of boundary conditions [12]. Their calculations suggest the spin current generated is constrained by the time for a carrier to diffuse across the sample and the spin relaxation time. Our focus is on the generation of more experimentally accessible charge currents. A similar system that has garnered interest is nonuniform spin-orbit interactions where spins are deflected in a Stern-Gerlach manner [15–18]. The prospect of generating spin or charge currents, via a spin-dependent interaction independent of the spin-orbit effect [19–25], is alluring as it offers up a wider variety of materials for inspection.

What will be demonstrated in this paper, by formulating and solving a system of spin and charge drift-diffusion equations, is that magnetic field gradients induce charge currents which are predicted to be measurable by a longitudinal voltage difference. One can view the original Stern-Gerlach experiment as an unpolarized beam generating a transverse spin current; here we propose a spin polarization generating a charge current—a process we term as the inverse Stern-Gerlach effect. After a general treatment of spin and charge drift diffusion equations with magnetic field gradients, the calculations described in this paper demonstrate the inverse Stern-Gerlach effect for the one-dimensional geometry shown in Fig. 1(a). This geometry is chosen for two reasons

(1) The magnetic field chosen, $\boldsymbol{B}(x,z) = \boldsymbol{B}_c + \boldsymbol{B}_\perp$, where $\boldsymbol{B}_c = bz\hat{z}$ and $\boldsymbol{B}_\perp = -bx\hat{x}$, is nondivergent and is an approximation for the inhomogeneous magnetic field either of the original Stern-Gerlach experiment or between four current carrying wires [6]. We choose a conducting one-dimensional channel to lie along $\hat{z}$; the field inside the channel is then $\boldsymbol{B}_c$ since $x = 0$ in the channel. Even when the velocity of a carrier is not completely constrained along $\hat{z}||\boldsymbol{B}_c$ or if $\boldsymbol{B}_\perp$ is finite within the channel, the Lorentz force is negated by the classical Hall effect.

(2) The second advantage gained by having the channel at $x = 0$ is that carriers injected into the channel with their spin along the magnetic field, $\boldsymbol{B}(0,z) = \boldsymbol{B}_c(z) + \boldsymbol{B}_\perp(0,z) = \boldsymbol{B}_c(z)$, will not precess. While the field, $\boldsymbol{B}_\perp$, is zero in the channel, the Stern-Gerlach force has two components due to the inhomogeneities along x and z as depicted in Fig. 1(a). Despite the transverse gradient along x being nonzero at $x = 0$, no transverse force is exerted on the spin ensemble due to the constrained geometry (motion only

*harmon.nicholas@gmail.com

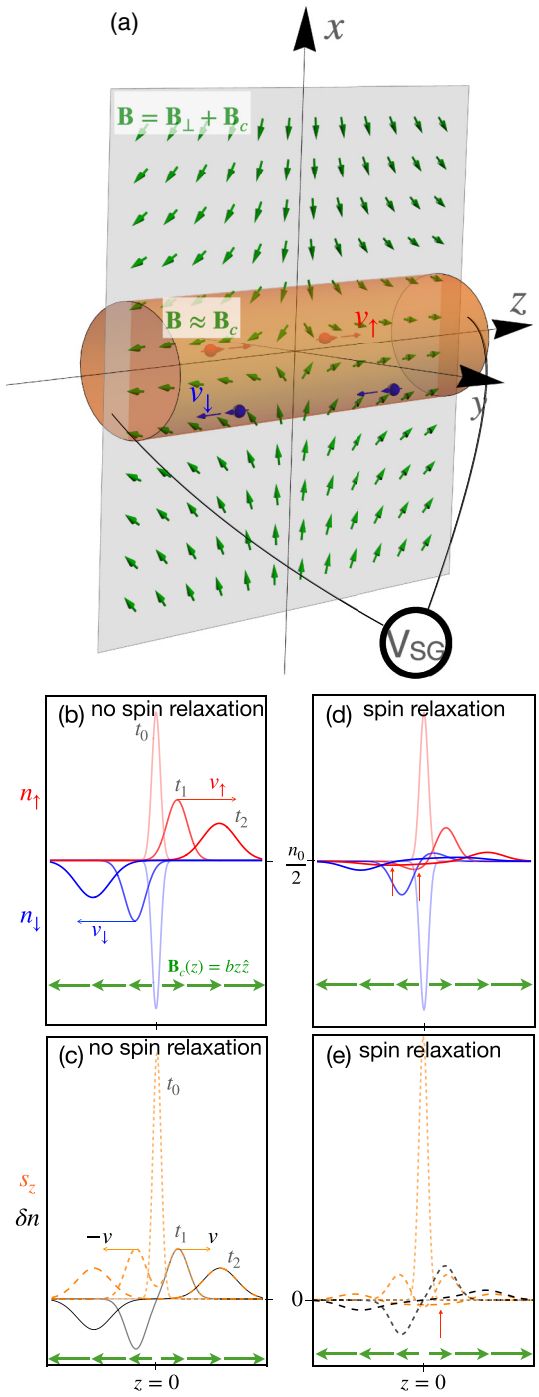

FIG. 1. (a) Geometry of a one-dimensional conductive channel in magnetic field, $\boldsymbol{B}(x,z) = bz\hat{z} - bx\hat{x}$. Within the channel, $\boldsymbol{B}(0,z) = \boldsymbol{B}_c$, which lies along the injected spin direction. Spin injection leads to deviations of up and down densities away from their equilibrium value $n_0/2$. Since $\boldsymbol{B}_c$ is nonuniform, there is a magnetic field gradient force causing spin up and spin down carrier densities to separate as shown in panel (b) for three different times after an initial Gaussian spin injection at the origin. (d, e) Identical to panels (b) and (c) except spin relaxation is included. (b–e) Insets: The nonuniform magnetic field $bz\hat{z}$ considered in this paper. Red arrows in panels (d) and (e) show presence of additional antinodes when spin relaxation is strong. Direction of packet motion is determined by νb which is chosen here as $\nu b < 0$. Ordinate quantities in panels (b)–(e) are per $\delta N_\uparrow/A$.

permitted along z). The term $bz\hat{z}$ does lead to a longitudinal force.

The force from the longitudinal gradient along z is the focus of this paper. Figure 1(b) displays transient responses of up/down spin densities, due to the longitudinal gradient, after a Gaussian impulse of spin density (at origin) in the absence of spin relaxation; unequal amounts of up and down spin travel in opposite directions leading to a charge current and voltage, $V_{\rm SG}$, across the length of the channel. Figure 1(c) depicts charge surplus (black line) moving to the right. The role spin relaxation plays [Figs. 1(d) and 1(e)] is subtle; aside from reducing amplitude as one might naturally expect, additional structure is formed (red arrows pointing to new local minima). We understand this phenomenon by analogy with the concept of countercurrent exchange [26] from the fields of physiology [27–30] and fluid/thermal dynamics [31–33].

II. SPIN AND CHARGE DRIFT-DIFFUSION EQUATIONS IN THE PRESENCE OF MAGNETIC FIELD GRADIENT

We approach the problem in a semiclassical manner by solving for spin-dependent velocities resulting from a Stern-Gerlach-like force generated by a nonuniform magnetic field. Given the magnetic moment of an electron, $\boldsymbol{\mu} = -\frac{1}{2}g^*\mu_B\boldsymbol{\sigma}$, and its dipole potential energy, $V = -\boldsymbol{\mu}\cdot\boldsymbol{B}$, we write a Stern-Gerlach force operator as

$$\hat{\boldsymbol{F}}_{\rm SG} = -\nabla V = -\tfrac{1}{2}g^*\mu_B\nabla(\boldsymbol{\sigma}\cdot\boldsymbol{B}). \tag{1}$$

The force is spin dependent—the force on $\uparrow$ / $\downarrow$ spins (z quantization axis) is $\boldsymbol{F}^{\uparrow/\downarrow}_{\rm SG} = \mp\frac{1}{2}g^*\mu_B\nabla B_z$. The inclusion of this force into a Drude-like model yields steady-state velocities:

$$\boldsymbol{v}^{\uparrow} = \frac{\boldsymbol{F}^{\uparrow}_{\rm SG}\tau}{m} = -\frac{g^*\mu_B\tau}{2m}\nabla B_z = -\nu\nabla B_z \tag{2}$$

where $\nu = \frac{g^*\mu_B\tau}{2m}$ has units of $\mathrm{m}^2/(\mathrm{T\ s})$ which we define as the *magnetic mobility* (in contrast to charge mobility), τ is the momentum relaxation time, m is the carrier mass, and g^* is the effective g factor. Note the velocity does not depend on the charge q in congruence with the force being moment and not charge dependent. The spin current is $\boldsymbol{j}^z_{{\rm SG},s} = \boldsymbol{j}^{\uparrow}_{\rm SG} - \boldsymbol{j}^{\downarrow}_{\rm SG} = -q(n_\uparrow + n_\downarrow)\nu\nabla B_z = -qn\nu\nabla B_z$ where n is the conduction charge density. Similarly for other directions of spin, the direction of spin couples to the same direction of magnetic field: $\boldsymbol{j}^i_{{\rm SG},s} = -qn\nu\nabla B_i$. We follow the same process for charge current: $\boldsymbol{j}_{{\rm SG},c} = -q\nu(s_x\nabla B_x + s_y\nabla B_y + s_z\nabla B_z)$ where s_i are components of spin density.

Following the usual prescription [34–38], the continuity equations for charge and spin are as follows:

$$\frac{\partial n}{\partial t} = -\frac{1}{q}\nabla\cdot\boldsymbol{j}_c, \tag{3}$$

$$\frac{\partial s_i}{\partial t} = -\frac{1}{q}\nabla\cdot\boldsymbol{j}^i_s - \frac{s_i}{\tau_s} + \mathrm{sgn}(q)\frac{g^*\mu_B}{\hbar}[\boldsymbol{s}\times\boldsymbol{B}(\boldsymbol{r})]_i \tag{4}$$

in which we substitute the following: diffusion ($\boldsymbol{j}_{\rm diff} = -qD\nabla n$), drift [$\boldsymbol{j}_{\rm drift} = \mathrm{sgn}(q)qn\mu\boldsymbol{E}$], and Stern-Gerlach ($\boldsymbol{j}_{{\rm SG},c}$) where $\mu = |q|\tau/m$ is the charge mobility, D is the diffusion constant, and τ_s is the spin relaxation time. Spin current versions for diffusion and drift are found by $n \to s_i$.

After inserting into the continuity equations we obtain a set of four coupled drift-diffusion equations for charge and spin:

$$\frac{\partial n}{\partial t} = D\nabla^2 n - \mathrm{sgn}(q)\mu[n\nabla\cdot\boldsymbol{E} + (\nabla n)\cdot\boldsymbol{E}] + \nu\sum_{i\in\{x,y,z\}}[(\nabla s_i)\cdot\nabla B_i(\boldsymbol{r}) + s_i\nabla^2 B_i(\boldsymbol{r})], \quad (5)$$

$$\frac{\partial s_i}{\partial t} = D\nabla^2 s_i - \mathrm{sgn}(q)\mu[s_i\nabla\cdot\boldsymbol{E} + (\nabla s_i)\cdot\boldsymbol{E}] - \frac{s_i}{\tau_s} + \nu[(\nabla n)\cdot\nabla B_i(\boldsymbol{r}) + n\nabla^2 B_i(\boldsymbol{r})] + \mathrm{sgn}(q)\frac{|g^*|\mu_B}{\hbar}[\boldsymbol{s}\times\boldsymbol{B}(\boldsymbol{r})]_i. \quad (6)$$

In two or three dimensions, the full $\boldsymbol{B}(x,z) = bz\hat{z} - bx\hat{x}$ must be used, which entails a complex dynamics between charge density and the three components of the spin density; it is only in one dimension where charge and a single component of spin density evolve if spin is initialized along $\boldsymbol{B}(0,z)$.

To understand the ramifications of the field gradient, in this paper we focus on the simplest case of one dimension (z) with electron carriers in a uniform electric field along z, an external magnetic field pointing along the one dimension such that $\boldsymbol{B}(z) = \boldsymbol{B}_c(z) = bz\hat{z}$ (a uniform field $B_0\hat{z}$ can be added but has no effect), and any injected spin being oriented along z as shown in Fig. 1(a). With these simplifications, Eqs. (5) and (6) reduce to

$$\frac{\partial n}{\partial t} = D\partial_z^2 n + \mu E_z\partial_z n + \nu b\partial_z s_z, \quad (7)$$

$$\frac{\partial s_z}{\partial t} = D\partial_z^2 s_z + \mu E_z\partial_z s_z + \nu b\partial_z n - \frac{s_z}{\tau_s}. \quad (8)$$

Boundary and initial conditions are determined by the specific experiment.

III. TRANSIENT SPIN DYNAMICS

In n-doped semiconductors, carriers can be spin polarized through methods of optical orientation [39]. To summarize the process, circularly polarized light excites partially spin-polarized electrons, n_{ex}, into the conduction band, which has equilibrium concentration $n_0 \gg n_{\mathrm{ex}}$. Conduction electrons rapidly recombine with conduction holes on a time scale $\tau_r << \tau_s$. Since there are more unpolarized electrons than polarized electrons, mostly unpolarized electrons recombine, which leaves a net spin density in the conduction band while the concentration of conduction electrons has returned to equilibrium, $n(0,z) = n_0$, after recombination [40]. It is after recombination, while a finite conduction spin density [$s_z(0,z) = 2\frac{S_0}{A}\delta(z)$] remains, that we consider our starting point as we solve Eqs. (7) and (8); $2S_0$ is the initial difference in spin up ($N_\uparrow$) and spin down ($N_\downarrow$) electrons and A is the cross-sectional area of the channel.

It is instructive to examine the time-dependent solutions to Eqs. (7) and (8) in terms of $n_{\uparrow,\downarrow}$, through the relations $n_\uparrow = (n+s_z)/2$ and $n_\downarrow = (n-s_z)/2$:

$$\frac{\partial n_\uparrow}{\partial t} = D\partial_z^2 n_\uparrow + \mu E_z\partial_z n_\uparrow + \nu b\partial_z n_\uparrow - \frac{n_\uparrow - n_\uparrow}{2\tau_s}, \quad (9)$$

$$\frac{\partial n_\downarrow}{\partial t} = D\partial_z^2 n_\downarrow + \mu E_z\partial_z n_\downarrow - \nu b\partial_z n_\downarrow - \frac{n_\downarrow - n_\uparrow}{2\tau_s}. \quad (10)$$

The coupling between $n_\uparrow$ and $n_\downarrow$ comes from spin-flip processes alone. When there is no spin relaxation, Appendix A shows the solutions for n and s are

$$n(t,z) = n_0 + \frac{S_0}{A}\frac{e^{-\frac{[z+(\nu b+\mu E_z)t]^2}{2(2Dt+\sigma^2)}} - e^{-\frac{[z+(-\nu b+\mu E_z)t]^2}{2(2Dt+\sigma^2)}}}{2\sqrt{2\pi}\sqrt{2Dt+\sigma^2}} \quad (11)$$

and

$$s_z(t,z) = \frac{S_0}{A}\frac{e^{-\frac{[z+(\nu b+\mu E_z)t]^2}{2(2Dt+\sigma^2)}} + e^{-\frac{[z+(-\nu b+\mu E_z)t]^2}{2(2Dt+\sigma^2)}}}{2\sqrt{2\pi}\sqrt{2Dt+\sigma^2}} \quad (12)$$

where σ is the width when the spin impulse is Gaussian. Figures 1(b) and 1(c) display these traveling Gaussian packets for up and down spin densities and s and n.

Figures 1(d) and 1(e) show the effects of spin relaxation: peaks are reduced as expected but also additional broad peaks form (e.g., at red arrows). This is further seen in Fig. 2(a) where a narrow peak quickly falls off while a much broader trailing peak rapidly forms and then slowly decays in time. At long times only these broad peaks remain [Fig. 2(a) inset]; $n_\uparrow$ and $n_\downarrow$ are approximately odd functions with peaks that slowly diminish. The peaks on either side of the origin move in opposite directions *for both* $n_\uparrow$ *and* $n_\downarrow$ in seeming contradiction to the Stern-Gerlach forces. The cause of this behavior can be understood by considering two up spins moving right. One flips and begins moving left (via Stern-Gerlach), separating from its partner. It may then flip again, causing it to move right but still trailing its partner. This process continues with the net result being what we observe in the Fig. 2(a) inset.

We find quantitative results by successive Fourier and Laplace transforms on Eqs. (7) and (8) or Eqs. (9) and (10) if D and impulse width are set to zero (which do not change the pertinent results). Appendix B provides details showing that, in the long-time limit,

$$\delta n_{\uparrow/\downarrow} = \frac{\delta N_\uparrow\, e^{-\frac{\gamma_s z^2}{4(\nu b)^2 t}}}{4A(\nu b)^2\sqrt{\pi}\, t^{3/2}}\left[-\mathrm{sgn}(\nu b)z\sqrt{\gamma_s} \pm \frac{\sqrt{\gamma_s}z^2}{2|\nu b|t} \mp \frac{|\nu b|}{\sqrt{\gamma_s}}\right] \quad (13)$$

or, when desiring to express the spin density,

$$s_z = \frac{e^{-\frac{\gamma_s(z+\mu E_z t)^2}{4(\nu b)^2 t}}}{2\sqrt{\pi}|\nu b|\sqrt{\gamma_s}\, t^{3/2}}\left(\frac{\gamma_s(z+\mu E_z t)^2}{2|\nu b|^2 t} - 1\right)\frac{\delta N_\uparrow}{A}. \quad (14)$$

From these results we find [see also Fig. 2(a) inset] the separation between the $n_\uparrow$ and $n_\downarrow$ peaks is $\approx 2|\nu b|\tau_s$; if spin relaxation is strong, flipped spins do not have time to backtrack so the $n_\uparrow$ and $n_\downarrow$ peaks coincide and the spin density is zero. The broad pulses also exist for s_z (dashed, orange); their peak positions are $z_s = \pm\sqrt{6t\tau_s}|\nu b|$, which suggests spin relaxation induces diffusivelike transport as spins flip between the up and down channels.

When an electric field is present, both spin species experience the same electric force, which acts like a change of reference frame for the spin packets. Figure 2(b) displays a transient where both the gradient force and electric force exist. Depending on the relative sizes of the two forces, the up and down spins move parallel or antiparallel to one another and move at different speeds (in the figure, down is faster than up).

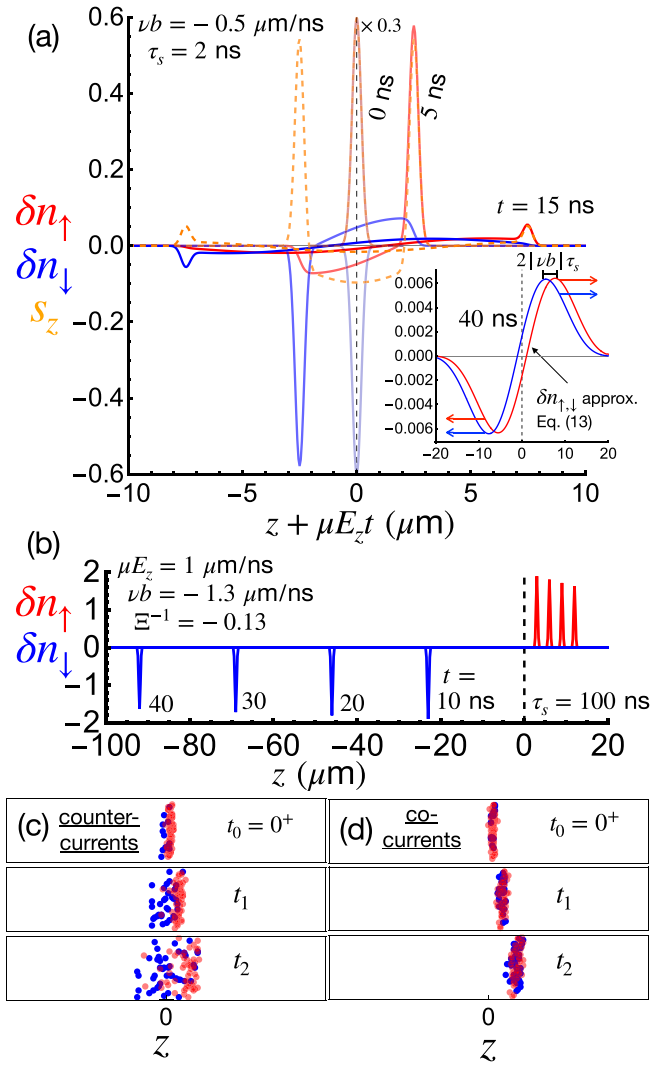

FIG. 2. (a) Examples of $\delta n_{\uparrow/\downarrow} = n_{\uparrow/\downarrow} - n_0/2$ and s_z carrier motion (up, red; down, blue; spin, orange) for moderate spin relaxation at four different times. The initial Gaussian peaks move ballistically but are reduced quickly due to spin relaxation. A slowly decaying, broad, shallow peak follows in its wake as spins flip back and forth. Inset: Up and down spins at longer time when the narrow peak has vanished. Left behind are broad diffusive peaks that maintain separation due to opposite Stern-Gerlach forces on them. (b) Temporal snapshots of $\delta n_{\uparrow/\downarrow}$ carrier motion for different combinations of μE_z and νb when spin relaxation is weak; up and down spin travel at different velocities depending on E_z and νb. Snapshots are after a Gaussian impulse, with width $\sigma = 0.2$ μm, at the origin. (c, d) Results, at three different instances, from Monte Carlo simulation of up spins (red) injected into a one-dimensional channel under the condition of (c) spin countercurrent exchange and (d) spin cocurrent exchange. Due to spin relaxation, up spins (red) convert to down spins (blue) and vice versa.

The interchannel diffusive behavior observed above in the Fig. 2(a) inset ($b \neq 0$ and $E_z = 0$) is not present when $b = 0$ and $E_z \neq 0$ where purely exponential in time behavior arises. We understand these contrasting phenomena by analogy with the concepts of cocurrent and countercurrent exchange [26] from the fields of physiology [27–30] and fluid/thermal dynamics [31,33]. Cocurrent/countercurrent exchange occurs when interacting bipartite flows are either parallel (co-) or antiparallel (counter-) to each other. One of many examples is oxygen transport between arterioles and venules where blood flows in opposite directions and diffusion of O_2 occurs between the microvessels; oxygen is transported quicker between the two microvessels when the blood flows are counter. Intuitively, countercurrent exchange can be thought of as more efficient than cocurrent exchange since to increase oxygen in a deficient vessel blood in that vessel should move toward the source (oxygen rich blood) and not away. The form of the differential equations used to model the oxygen partial pressure of the microvessels is identical to Eqs. (9) and (10) [41]. Another example, elaborated in Appendix C, is fish respiration where intake water flows opposite to blood flow in order to maximize blood oxygenation. The flow of up and down spins is analogous where the exchange process is spin flips between up and down spin channels.

Figures 2(c) and 2(d) are Monte Carlo simulations of countercurrent (c) and cocurrent exchange (d) where the red and blue filled circles represent up and down spins that flow in directions dictated by the magnetic gradient and electric field. All spins are initially up at the origin. The gradient field causes a rapid spreading of the packet since spin flips induce opposite spins to move apart. The electric field drives each spin in the same direction, which reduces the packet's spreading since spin flips do not force separation of opposite spins. Figures 2(c) and 2(d) make this apparent: the up and down spin populations separate from one another for pure countercurrents ($E_z = 0$) in Fig. 2(c), which means a down spin is unlikely to contribute to the primary packet when it flips back up. For cocurrent exchange ($b = 0$) in Fig. 2(d), spin flips are less severe as up and down spins stay proximal so the packet's integrity is maintained over longer distance.

IV. STEADY STATE

We also consider continuous optical pumping of spin into the conduction band [39,42] to determine steady-state spin and charge concentrations:

$$0 = D\partial_z^2 n + \mu E_z \partial_z n + \nu b \partial_z s_z, \tag{15}$$

$$0 = D\partial_z^2 s_z + \mu E_z \partial_z s_z + \nu b \partial_z n - \frac{s_z}{\tau_s} + 2g\delta(z), \tag{16}$$

where g is the rate per cross-sectional area of continuously injected nonequilibrium spins at the origin. The solutions of Eqs. (15) and (16) can be written, when $E_z = 0$, in the following form:

$$s_z = g\tau_s \frac{e^{-\frac{|z|}{\ell_0^2}\sqrt{(\ell_b^2+\ell_0^2)}}}{\sqrt{\ell_b^2+\ell_0^2}}, \tag{17}$$

$$\delta n = \mathrm{sgn}(z\nu b)\ell_b \frac{s_z - \frac{g\tau_s}{\sqrt{\ell_b^2+\ell_0^2}}}{\sqrt{\ell_b^2+\ell_0^2}} \tag{18}$$

where $\ell_0 = \sqrt{D\tau_s}$ is the spin diffusion length and $\ell_b = |\nu b|\tau_s$ is the magnetic gradient drift length. When $\ell_b \gg \ell_0$, the diffusion lengths become $\ell_0^2/\ell_b = D/|\nu b|$, which explains the

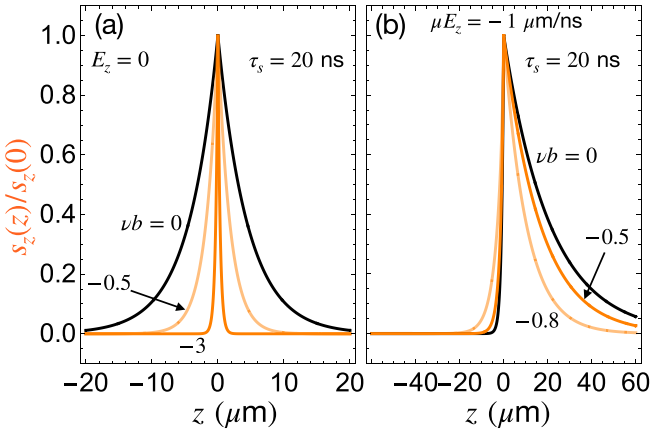

FIG. 3. Calculations of steady-state spin density in the (a) absence, using Eq. (17), and (b) presence of a uniform electric field for different field gradients; the black curve ($\nu b = 0$) is Eq. (19). A delta source of spin injection at the origin is assumed. (a), (b) Curves are normalized to demonstrate how b influences spin decay length.

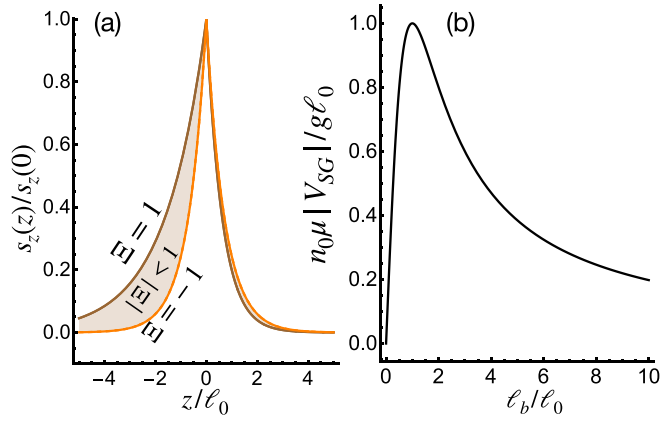

FIG. 4. (a) Allowable steady-state normalized spin density region for possible spin countercurrent exchange parameters, Ξ, for $\tau_s' = D' = 1$. The brown (orange) line denotes spin cocurrent (countercurrent) exchange given by Eqs. (17) and (19). The influence of countercurrent exchange is to reduce the (longer) downstream spin diffusion length and slightly increase the (much shorter) upstream spin diffusion length. (b) Predicted dependence of Stern-Gerlach voltage, $V_{\rm SG}$, on magnetic gradient length, ℓ_b.

behavior for spin decay lengths seen in Fig. 3(a) for three values of the magnetic field gradient. Though spin-flip coupling between the two channels (up and down) is the same for all three, when $\nu b \neq 0$, the transport length is severely suppressed due to spin countercurrent exchange.

Without the gradient field but with the electric field turned on, s_z is uncoupled to n, and after a delta impulse the time-dependent solution for $s_z(t)$ is one in which a diffusive packet drifts at speed μE_z while also undergoing exponential spin relaxation, e^{-t/τ_s}. In the steady state,

$$s_z = g\tau_s \frac{e^{-\mathrm{sgn}(E_z)\frac{\ell_d}{\ell_0}\frac{z}{\ell_0} - \sqrt{4\ell_0^2+\ell_d^2}\frac{|z|}{2\ell_0^2}}}{\sqrt{\ell_d^2+\ell_0^2}} \tag{19}$$

where $\ell_d = \mu|E_z|\tau$ is the spin drift length. There are two decay lengths (upstream and downstream), as found by [43], characterizing the black curves in Fig. 3(b). The electric field supplies an identical force to both spins, which is indicative of a cocurrent.

Inclusion of the gradient and electric fields leads to a situation between purely countercurrent and cocurrent exchange. In Fig. 3(b), the gradient field suppresses the downstream transport length ($z > 0$) but enhances the much shorter upstream length ($z < 0$). To analyze the effects of countercurrent exchange for any b and E_z, we rewrite the drift-diffusion equations for $n_{\uparrow,\downarrow}$ in dimensionless form:

$$\frac{\partial n_\uparrow}{\partial t'} = D'\partial_{z'}^2 n_\uparrow + \partial_{z'} n_\uparrow - \frac{n_\uparrow - n_\uparrow}{2\tau_s'}, \tag{20}$$

$$\frac{\partial n_\downarrow}{\partial t'} = D'\partial_{z'}^2 n_\downarrow + \Xi\partial_{z'} n_\downarrow - \frac{n_\downarrow - n_\uparrow}{2\tau_s'} \tag{21}$$

where $t' = t(\mu E_z + \nu b)/\ell_0$, $D' = D/\ell_0(\mu E_z + \nu b)$, $\tau_s' = \tau_s(\mu E_z + \nu b)/\ell_0$, and $z' = z/\ell_0$ are dimensionless units; $\Xi = \frac{\mu E_z - \nu b}{\mu E_z + \nu b}$ is the spin countercurrent exchange parameter, which gives the degree of opposition present between up and down spin currents; and μE_z and νb are assumed to have the same sign. Appendix E provides the same equations but for n and s. $\Xi = 1$ ($b = 0$) implies pure spin cocurrent exchange [34,43,44], and $\Xi = -1$ ($E_z = 0$) implies pure spin countercurrent exchange. When both electric and gradient fields are present an intermediate situation exists where $-1 < \Xi < 1$. Figure 4(a) shows any deviation from purely cocurrent conditions (black line) reduces the downstream spin diffusion length; the strongest suppression occurs for purely countercurrent exchange (orange line). Consideration of countercurrent exchange should be made when interpreting spin transport experiments where magnetic field gradients are known to exist [45–47].

V. STERN-GERLACH POTENTIAL DIFFERENCE

Although the magnetic field gradient may be an obstacle for spin transport, it nevertheless does give rise to a Stern-Gerlach charge current $\boldsymbol{j}_{\mathrm{SG},c}$. The potential difference across the sample is found by considering the Stern-Gerlach force as an effective electric force such that $\boldsymbol{j}_{\mathrm{SG},c} = \sigma_c \boldsymbol{E}_{\mathrm{eff}}$ where $\sigma_c = |q|\mu n$ is the charge conductivity. We then write $\Delta V_{\rm SG} = \int_{-\infty}^{\infty} \frac{j_{\mathrm{SG},c}}{\sigma_c} dz$. With an electric field absent, we use s_z of Eq. (17) to obtain

$$|\Delta V_{\rm SG}| = \frac{2g}{\mu n_0}\ell_b \frac{\ell_0^2}{\ell_0^2+\ell_b^2} \tag{22}$$

where we use $n \approx n_0$ since $n_0 \gg \delta n$. Figure 4(b) demonstrates the relationship between $\Delta V_{\rm SG}$ and the magnetic gradient drift length. Voltage is maximum when $\ell_0 = \ell_b$; under such a condition, the voltage scales as ℓ_b. No dependence on the excitation pulse width σ is found, as shown in Appendix F. In general, $|\Delta V_{\rm SG}|$ depends on E_z through s_z. A detailed analysis of the voltage dependence on electric field is a subject for future work.

To estimate the potential we consider $g = s_{\rm ex} f$ as the rate of generated spins per cross-sectional area. We approximate the excited cross-sectional spin density as $(10^{14}\ \mathrm{cm}^{-3})^{2/3} \approx 10^9\ \mathrm{cm}^{-2}$ and use a pump repetition rate

$f \approx 100$ MHz [43,48]. A typical spin diffusion length in GaAs is 10 μm [49,50]. Using $\mu = 1000$ cm^2/V s and $n_0 \approx 10^{16}$ cm^{-3}, the maximum voltage is ≈10 μV, which is well within the range of measurement [51]. To achieve $\ell_b = \ell_0 \approx 10$ μm, b would need to be ≈10^6 T/m, which is large but comparable gradients have been produced by the stray fields of certain patterned magnetic films [52–54]. Rashba-field gradients offer even larger gradients ≈10^8 T/m, which have been used to produce spin separation in InAs quantum point contacts [17]. Smaller, though still significant, are gradients produced by spin polarized nuclei [37,39,45,55,56]. Advantages to these latter two are avoidance of Lorentz forces in two or three dimensions and, if appropriately oriented, avoidance of spin precession effects.

VI. CONCLUSION

The force of magnetic field gradients on conduction spin magnetic moments has been incorporated into a series of spin and charge drift-diffusion equations. We suggest an optical approach to measure an appreciable voltage difference generated by spin and charge dynamics in the magnetic gradient. The predicted Stern-Gerlach voltage, in competition with an inverse Spin Hall voltage, may also be measured electrically in a two-dimensional geometry where a gradient field is transverse to a spin current. A full analysis in two or three dimensions is needed due to the necessity of spin precession in higher dimension. A reported dependence of potential on dynamically polarized nuclei is suggestive of this inverse Stern-Gerlach effect [57].

ACKNOWLEDGMENTS

This work was supported by NSF Grants No. DMR-2014786 and No. DMR-2152540.

APPENDIX A: TIME-DEPENDENT SOLUTIONS

Our initial conditions are $n(0,z) = n_0$ and $s_z(0,z) = 2\frac{S_0}{A}\delta(z)$. The solutions for n and s_z can be later convolved with a more realistic Gaussian injection pulse of width σ. The $2S_0$ comes from $2S_0 = N_\uparrow - N_\downarrow = (\frac{N_0}{2} + \delta N_\uparrow) - (\frac{N_0}{2} + \delta N_\downarrow) = (\frac{N_0}{2} + \delta N_\uparrow) - (\frac{N_0}{2} - \delta N_\uparrow) = 2\delta N_\uparrow$ where A is the cross-sectional area of the quasi-one-dimensional system and $\delta N_\uparrow = N_\uparrow - N_0/2$. So the factor of 2 is coming from the number of surplus up spins injected being equal to the number of deficit down spins. The Fourier transforms, $\hat{f}(k) = \frac{1}{\sqrt{2\pi}}\int_{-\infty}^{\infty} f(z)e^{-ikz}dk$, for these initial conditions are $\sqrt{2\pi}n_0\delta(k)$ and $\frac{2}{\sqrt{2\pi}}\frac{S_0}{A}$ for charge and spin, respectively.

When spin relaxation is not present, the up and down spin equations are two independent partial differential equations with solutions shown in Figs. 1(b) and 1(c). Equations (5) and (6) can be solved exactly when there is no spin relaxation. Taking the Fourier transform of Eqs. (5) and (6) leads to

$$\frac{\partial \hat{n}}{\partial t} = -k^2 D\hat{n} + ik(\nu b\hat{s}_z + \mu E_z\hat{n}), \tag{A1}$$

$$\frac{\partial \hat{s}_z}{\partial t} = -k^2 D\hat{s}_z + ik(\nu b\hat{n} + \mu E_z\hat{s}_z), \tag{A2}$$

or in the spin up and down picture

$$\frac{\partial \hat{n}_\uparrow}{\partial t} = -k^2 D\hat{n}_\uparrow - ik(\nu b\hat{n}_\uparrow + \mu E_z\hat{n}_\uparrow), \tag{A3}$$

$$\frac{\partial \hat{n}_\downarrow}{\partial t} = -k^2 D\hat{n}_\downarrow + ik(\nu b\hat{n}_\downarrow + \mu E_z\hat{n}_\downarrow). \tag{A4}$$

The solutions to these now ordinary differential equations are

$$\hat{n}(t,k) = [\hat{n}(0,k)\cos(\nu bkt) + i\hat{s}_z(0,k)\sin(\nu bkt)] \times e^{-k^2Dt}e^{ik\mu E_z t}, \tag{A5}$$

$$\hat{s}_z(t,k) = [\hat{n}(0,k)\sin(\nu bkt) + i\hat{s}_z(0,k)\cos(\nu bkt)] \times e^{-k^2Dt}e^{ik\mu E_z t}. \tag{A6}$$

After inserting the initial conditions in Fourier space, we use the inverse Fourier transform ($f(z) = \frac{1}{\sqrt{2\pi}}\int_{-\infty}^{\infty}\hat{f}(k)e^{ikz}dk$) to obtain the following solutions:

$$n(t,z) = n_0 + \frac{S_0}{A}\frac{e^{-\frac{[z+(\nu b+\mu E_z)t]^2}{4Dt}} - e^{-\frac{[z+(-\nu b+\mu E_z)t]^2}{4Dt}}}{4\sqrt{\pi Dt}} \tag{A7}$$

and

$$s_z(t,z) = \frac{S_0}{A}\frac{e^{-\frac{[z+(\nu b+\mu E_z)t]^2}{4Dt}} + e^{-\frac{[z+(-\nu b+\mu E_z)t]^2}{4Dt}}}{4\sqrt{\pi Dt}}, \tag{A8}$$

which in either case are seen to consist of two diffusive wave packets moving at velocities $\pm\nu b + \mu E_z$ in the z direction.

For a Gaussian impulse of width σ, convolution yields

$$n(t,z) = n_0 + \frac{S_0}{A}\frac{e^{-\frac{[z+(\nu b+\mu E_z)t]^2}{2(2Dt+\sigma^2)}} - e^{-\frac{[z+(-\nu b+\mu E_z)t]^2}{2(2Dt+\sigma^2)}}}{2\sqrt{2}\pi\sqrt{2Dt+\sigma^2}} \tag{A9}$$

and

$$s_z(t,z) = \frac{S_0}{A}\frac{e^{-\frac{[z+(\nu b+\mu E_z)t]^2}{2(2Dt+\sigma^2)}} + e^{-\frac{[z+(-\nu b+\mu E_z)t]^2}{2(2Dt+\sigma^2)}}}{2\sqrt{2}\pi\sqrt{2Dt+\sigma^2}}. \tag{A10}$$

APPENDIX B: LONG-TIME LIMIT FOR SPIN AND CHARGE DENSITIES

Equations (7) and (8) written in terms of up and down spin densities are

$$\frac{\partial n_\uparrow}{\partial t} = D\partial_z^2 n_\uparrow + \mu E_z\partial_z n_\uparrow + \nu b\partial_z n_\uparrow - \frac{n_\uparrow - n_\uparrow}{2\tau_s}, \tag{B1}$$

$$\frac{\partial n_\downarrow}{\partial t} = D\partial_z^2 n_\downarrow + \mu E_z\partial_z n_\downarrow - \nu b\partial_z n_\downarrow - \frac{n_\downarrow - n_\uparrow}{2\tau_s} \tag{B2}$$

through the use of $n_\uparrow = (n + s_z)/2$ and $n_\downarrow = (n - s_z)/2$. Dual Fourier and Laplace transformations of these equations yield

$$s\tilde{\hat{n}}_\uparrow + \frac{n_0}{2}\sqrt{2\pi}\delta(k) + \frac{\delta N_\uparrow e^{-\frac{\sigma^2k^2}{2}}}{\sqrt{2\pi}A} = -k^2D\tilde{\hat{n}}_\uparrow - ik(\nu b\tilde{\hat{n}}_\uparrow + \mu E_z\tilde{\hat{n}}_\uparrow) - \frac{\tilde{\hat{n}}_\uparrow - \tilde{\hat{n}}_\downarrow}{2\tau_s}, \tag{B3}$$

$$s\tilde{\hat{n}}_\downarrow + \frac{n_0}{2}\sqrt{2\pi}\delta(k) - \frac{\delta N_\uparrow e^{-\frac{\sigma^2k^2}{2}}}{\sqrt{2\pi}A} = -k^2D\tilde{\hat{n}}_\downarrow + ik(\nu b\tilde{\hat{n}}_\downarrow + \mu E_z\tilde{\hat{n}}_\downarrow) - \frac{\tilde{\hat{n}}_\downarrow - \tilde{\hat{n}}_\uparrow}{2\tau_s}. \tag{B4}$$

From this we find solutions in the Fourier-Laplace spaces to be

$$\tilde{\hat{n}}_{\uparrow/\downarrow} = \frac{n_0}{2}\sqrt{2\pi}\delta(k) \pm \delta N_\uparrow \frac{e^{-\frac{1}{2}k^2\sigma^2}}{\sqrt{2\pi}} \frac{Dk^2 \pm i\nu bk + s}{(\nu b)^2k^2 + (Dk^2+s)(Dk^2+\gamma_s+s)} \tag{B5}$$

where we have substituted $E_z = 0$ for the time being. Constant electric field can be added later by simply $z \to z + \mu E_z t$.

To perform the inverse Fourier transform, $f(z) = \frac{1}{\sqrt{2\pi}}\int_{-\infty}^{\infty}\hat{f}(k)e^{ikz}dk$, we need to assume a delta initial condition so $\sigma = 0$ and no diffusion ($D = 0$). To retain a Gaussian initial condition, one can perform a convolution later. The inverse Fourier transform delivers

$$\tilde{n}_{\uparrow/\downarrow} = \frac{n_0}{2s} \pm \frac{\delta N_\uparrow}{2A(\nu b)^2} e^{-|z|\frac{\sqrt{s(s+\gamma_s)}}{|\nu b|}} \left(s\frac{|\nu b|}{\sqrt{s(s+\gamma_s)}} \mp \nu b\,\mathrm{sgn}(z)\right). \tag{B6}$$

One approximation is to assume a fast spin relaxation, or equivalently the long-time (small s) limit, such that

$$\tilde{n}_{\uparrow/\downarrow} \approx \frac{n_0}{2s} \pm \frac{\delta N_\uparrow}{2A(\nu b)^2} e^{-|z|\frac{\sqrt{s\gamma_s}}{|\nu b|}} \left(\frac{|\nu b|\sqrt{s}}{\sqrt{\gamma_s}} \mp \nu b\,\mathrm{sgn}(z)\right), \tag{B7}$$

which has an inverse Laplace transform that can be performed analytically:

$$\begin{aligned} n_{\uparrow/\downarrow} &= \frac{n_0}{2} + \frac{\delta N_\uparrow\, e^{-\frac{\gamma_s z^2}{4(\nu b)^2 t}}}{4A(\nu b)^2\sqrt{\pi}\, t^{3/2}} \\ &\quad\times \left[-\mathrm{sgn}(\nu b) z\sqrt{\gamma_s} \pm \frac{\sqrt{\gamma_s} z^2}{2|\nu b| t} \mp \frac{|\nu b|}{\sqrt{\gamma_s}}\right] \\ &= \frac{n_0}{2} + \delta n_{\uparrow/\downarrow}. \end{aligned} \tag{B8}$$

From these expressions, Eq. (14) and

$$\delta n = \delta n_\uparrow + \delta n_\downarrow = -\mathrm{sgn}(\nu b)\frac{\sqrt{\gamma_s}(z+\mu E_z t)e^{-\frac{\gamma_s(z+\mu E_z t)^2}{4(\nu b)^2 t}}}{2A\sqrt{\pi}|\nu b|^2\, t^{3/2}}\delta N_\uparrow \tag{B9}$$

are ascertained.

The two asymptotic spin accumulation pulses have peak positions $z_s = \pm\sqrt{6t\tau_s}|\nu b|$. The two asymptotic charge accumulation/deficit pulses have peak positions $z_n = \pm\sqrt{2t\tau_s}|\nu b|$. The broad peak heights decay differently as well; the spin peaks according to $1/(2\,e^{3/2}\,\sqrt{\pi\gamma_s}\,|\nu b|\,t^{3/2})$ and the charge peaks according to $-\mathrm{sgn}(\nu b)/(2\,e^{1/2}\,\sqrt{2\pi}\,|\nu b|\,t)$. The separation between the peaks stays nearly constant at $2|\nu b|\tau_s$. On timescales much shorter than $1/\gamma_s$, the narrow peak amplitude decays with a rate $\gamma_s/2$ for nonzero νb whereas the rate is γ_s if $\nu b = 0$.

APPENDIX C: COUNTERCURRENT EXCHANGE IN FISH RESPIRATION

An example of countercurrent exchange is fish respiration where O_2 rich water flows between gill filament lamellae as shown in Fig. 5. Gas exchange occurs in the lamellae as CO_2 in blood is exchanged for O_2 in the water. In this manner, oxygen enters the bloodstream. The exchange is efficient because the blood flows through the lamellae opposite to the flow of water. Intuitively, countercurrent exchange can be thought of as more efficient than cocurrent exchange since to increase oxygen deficient blood should move toward the source of oxygen (countercurrent) and not away (cocurrent).

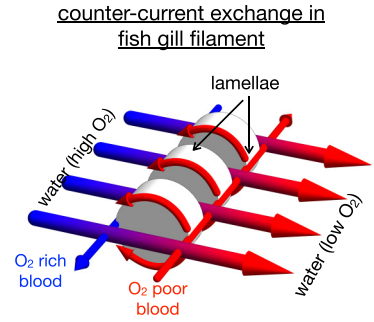

FIG. 5. Example of countercurrent exchange of CO_2 and O_2 in fish gills.

APPENDIX D: STEADY-STATE SOLUTIONS

We seek out solutions to

$$0 = D\partial_z^2 n + \mu E_z \partial_z n + \nu b\partial_z s_z, \tag{D1}$$

$$0 = D\partial_z^2 s_z + \mu E_z \partial_z s_z + \nu b\partial_z n - \frac{s_z}{\tau_s} + 2g\delta(z) \tag{D2}$$

where g is the rate per cross-sectional area of continuously injected nonequilibrium spins at the origin. Solutions are obtained using the Fourier transform method or elementary methods for second order ordinary differential equations.

Note that the charge deviation, found from these equations, does not decay to zero at large z. However, the charge deviation δn is expected to be minuscule compared to equilibrium charge density, n_0.

Figure 6 shows how the magnetic field gradient (or countercurrent exchange) affects the up and down spin densities under the same conditions as in Fig. 3(a). In the presence of the gradient field, spin-flip coupling ties the up and down spin channels together and the spin diffusion length is drastically shortened.

APPENDIX E: COUNTERCURRENT EXCHANGE PARAMETER

The equations of the main text

$$\frac{\partial n_\uparrow}{\partial t'} = D'\partial_{z'}^2 n_\uparrow + \partial_{z'} n_\uparrow - \frac{n_\uparrow - n_\uparrow}{2\tau_s'}, \tag{E1}$$

$$\frac{\partial n_\downarrow}{\partial t'} = D'\partial_{z'}^2 n_\downarrow + \Xi\partial_{z'} n_\downarrow - \frac{n_\downarrow - n_\uparrow}{2\tau_s'} \tag{E2}$$

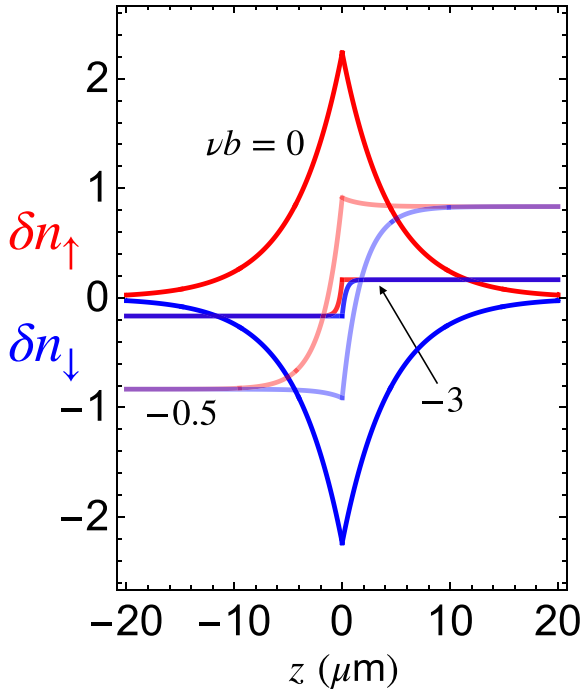

FIG. 6. Equivalent to Fig. 3(a) except in terms of $\delta n_\uparrow$ and $\delta n_\downarrow$ variables. The ordinate quantities are per g, the spin injection rate per cross-sectional area.

can be written in terms of s_z and n as

$$\frac{\partial s_z}{\partial t'} = D'\partial_{z'}^2 s_z + \frac{1}{2}(1+\Xi)\partial_{z'} s_z + \frac{1}{2}(1-\Xi)\partial_{z'} n - \frac{s_z}{\tau_s'}, \quad \text{(E3)}$$

$$\frac{\partial n}{\partial t'} = D'\partial_{z'}^2 n + \frac{1}{2}(1+\Xi)\partial_{z'} n + \frac{1}{2}(1-\Xi)\partial_{z'} s_z. \quad \text{(E4)}$$

If μE_z and μb are opposite signs, the dimensionless equations are expressed as

$$\frac{\partial n_\uparrow}{\partial t'} = D'\partial_{z'}^2 n_\uparrow + \Xi^{-1}\partial_{z'} n_\uparrow - \frac{n_\uparrow - n_\uparrow}{2\tau_s'}, \quad \text{(E5)}$$

$$\frac{\partial n_\downarrow}{\partial t'} = D'\partial_{z'}^2 n_\downarrow + \partial_{z'} n_\downarrow - \frac{n_\downarrow - n_\uparrow}{2\tau_s'} \quad \text{(E6)}$$

where $t' = t(\mu E_z - \nu b)/\ell_0$; $D' = D/\ell_0(\mu E_z - \nu b)$, $\tau_s' = \tau_s(\mu E_z - \nu b)/\ell_0$, and $z' = z/\ell_0$ are dimensionless units; $\Xi^{-1} = \frac{\mu E_z + \nu b}{\mu E_z - \nu b}$ gives the degree of opposition present between up and down spin currents; and μE_z and νb are assumed to have opposite signs.

Figure 7 shows plots of up and down spin for different values of Ξ at different snapshots in time. $\Xi > 0$ implies a partially cocurrent exchange process occurring while $\Xi < 0$ implies a partially countercurrent exchange process.

APPENDIX F: EFFECT OF OPTICAL PULSE WIDTH ON V_{SG}

If g is the rate per cross-sectional area of continuously injected nonequilibrium spins at the origin $[2g\delta(z)/A]$, the solutions can be written in the following compact

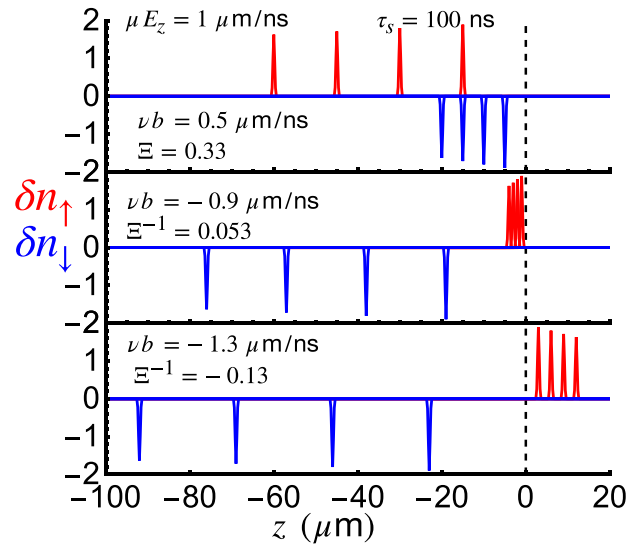

FIG. 7. Examples of $\delta n_{\uparrow/\downarrow} = n_{\uparrow/\downarrow} - n_0/2$ carrier motion for different countercurrent exchange parameters, Ξ, when spin relaxation is weak; up and down spin travel at different speeds depending on E_z and νb. Snapshots are at times 10, 20, 30, and 40 ns after a Gaussian impulse, with width $\sigma = 0.2$ μm, at the origin. Ordinate quantities are per $\delta N_\uparrow/A$ where $\delta N_\uparrow = N_\uparrow - N_0/2$.

form:

$$s_z = g\tau_s \frac{e^{-\frac{|z|}{\ell_0^2}\sqrt{(\ell_b^2+\ell_0^2)}}}{\sqrt{\ell_b^2+\ell_0^2}}, \quad \text{(F1)}$$

$$\delta n = g\tau_s \mathrm{sgn}(\nu b)\ell_b \frac{e^{-\frac{|z|}{\ell_0^2}\sqrt{\ell_b^2+\ell_0^2}} - 1}{\ell_b^2+\ell_0^2}\mathrm{sgn}(z) \quad \text{(F2)}$$

where $\ell_0 = \sqrt{D\tau_s}$ is the spin diffusion length and $\ell_b = |\nu b|\tau_s$ is the magnetic gradient drift length. If a more realistic Gaussian impulse is used, the solution is a convolution:

$$s_z \to \int_{-\infty}^{\infty} s_z(z')\frac{1}{\sqrt{2\pi\sigma^2}} e^{-\frac{(z-z')^2}{2\sigma^2}} dz'$$

$$= \frac{g\tau_s}{2\sqrt{\ell_b^2+\ell_0^2}}\left[e^{-\frac{z}{\ell}+\frac{\sigma^2}{2\ell^2}}\mathrm{erfc}\left(\frac{-z+\sigma^2/\ell}{\sqrt{2}\sigma}\right)\right.$$

$$\left. + e^{\frac{z}{\ell}+\frac{\sigma^2}{2\ell^2}}\mathrm{erfc}\left(\frac{z+\sigma^2/\ell}{\sqrt{2}\sigma}\right)\right] \quad \text{(F3)}$$

where $\ell = \ell_0^2/\sqrt{\ell_b^2+\ell_0^2}$.

We then write $\Delta V_{SG} = \int_{-\infty}^{\infty} \frac{j_{SG,c}}{\sigma_c} dz = -\int_{-\infty}^{\infty} \frac{s_z q \nu b}{\sigma_c} dz$ and substitute in

$$s_z = \frac{g\tau_s}{2\sqrt{\ell_b^2+\ell_0^2}}\left[e^{-\frac{z}{\ell}+\frac{\sigma^2}{2\ell^2}}\mathrm{erfc}\left(\frac{-z+\sigma^2/\ell}{\sqrt{2}\sigma}\right)\right.$$

$$\left. + e^{\frac{z}{\ell}+\frac{\sigma^2}{2\ell^2}}\mathrm{erfc}\left(\frac{z+\sigma^2/\ell}{\sqrt{2}\sigma}\right)\right] \quad \text{(F4)}$$

or

$$s_z = \frac{g\tau_s}{2\sqrt{\ell_b^2+\ell_0^2}} e^{\frac{\sigma^2}{2\ell^2}} \left[e^{-\frac{z}{\ell}} \mathrm{erfc}\left(\frac{-z+\sigma^2/\ell}{\sqrt{2}\sigma} \right) + e^{\frac{z}{\ell}} \mathrm{erfc}\left(\frac{z+\sigma^2/\ell}{\sqrt{2}\sigma} \right) \right]. \tag{F5}$$

The integral $\int_{-\infty}^{\infty} s_z dz$ becomes

$$\frac{g\tau_s}{2\sqrt{\ell_b^2+\ell_0^2}} e^{\frac{\sigma^2}{2\ell^2}} \int_{-\infty}^{\infty} \left[e^{-\frac{z}{\ell}} \mathrm{erfc}\left(\frac{-z+\sigma^2/\ell}{\sqrt{2}\sigma} \right) + e^{\frac{z}{\ell}} \mathrm{erfc}\left(\frac{z+\sigma^2/\ell}{\sqrt{2}\sigma} \right) \right] dz. \tag{F6}$$

Making a change of variable $z' = z/\sqrt{2}\sigma$ yields

$$\frac{g\tau_s}{2\sqrt{\ell_b^2+\ell_0^2}} e^{\frac{\sigma^2}{2\ell^2}} \int_{-\infty}^{\infty} \left[e^{-\frac{\sqrt{2}\sigma z'}{\ell}} \mathrm{erfc}\left(-z' + \frac{\sigma/\ell}{\sqrt{2}} \right) + e^{\frac{\sqrt{2}\sigma z'}{\ell}} \mathrm{erfc}\left(z' + \frac{\sigma/\ell}{\sqrt{2}} \right) \right] \sqrt{2}\sigma dz', \tag{F7}$$

which MATHEMATICA 13.2 simplifies as

$$\frac{g\tau_s}{\sqrt{\ell_b^2+\ell_0^2}} 2\ell. \tag{F8}$$

The Stern-Gerlach voltage is then

$$|\Delta V_{\mathrm{SG}}| = \int_{-\infty}^{\infty} \frac{s_z \nu b}{\mu n} dz = \frac{\nu b}{\mu n} \frac{g\tau_s}{\sqrt{\ell_b^2+\ell_0^2}} 2\ell = \frac{2\ell_b}{\mu n} \frac{g}{\sqrt{\ell_b^2+\ell_0^2}} \ell = \frac{2\ell_b}{\mu n} g \frac{\ell_0^2}{\ell_b^2+\ell_0^2}, \tag{F9}$$

which is the same result we had when σ was zero. Thus we find that the width of the Gaussian spin excitation pulse will not occlude the Stern-Gerlach signal.

[1] W. Gerlach and O. Stern, Z. Phys. **9**, 353 (1922).
[2] W. Gerlach and O. Stern, Z. Phys. **8**, 110 (1922).
[3] R. G. Fraser, Proc. R. Soc. A **114**, 212 (1927).
[4] L. Brillouin, Comptes Rendus, Acad. Sci. Paris **184**, 82 (1927).
[5] L. Brillouin, Proc. Natl. Acad. Sci. USA **14**, 755 (1928).
[6] B. Garraway and S. Stenholm, Contemp. Phys. **43**, 147 (2002).
[7] B. M. Garraway and S. Stenholm, Phys. Rev. A **60**, 63 (1999).
[8] G. A. Gallup, H. Batelaan, and T. J. Gay, Phys. Rev. Lett. **86**, 4508 (2001).
[9] N. F. Mott, Proc. R. Soc. A **124**, 425 (1929).
[10] J. Kessler, *Polarized Electrons* (Springer, New York, 1985), Vol. 1.
[11] J. Fabian, A. Abiague, C. Ertler, P. Stano, and I. Zutic, Acta Phys. Slovaca **57** (2007).
[12] J. Fabian and S. Das Sarma, Phys. Rev. B **66**, 024436 (2002).
[13] I. Martin, Phys. Rev. B **67**, 014421 (2003).
[14] J. Wróbel, T. Dietl, A. Łusakowski, G. Grabecki, K. Fronc, R. Hey, K. H. Ploog, and H. Shtrikman, Phys. Rev. Lett. **93**, 246601 (2004).
[15] J. I. Ohe, M. Yamamoto, T. Ohtsuki, and J. Nitta, Phys. Rev. B **72**, 041308(R) (2005).
[16] A. Pályi, C. Péterfalvi, and J. Cserti, Phys. Rev. B **74**, 073305 (2006).
[17] M. Kohda, S. Nakamura, Y. Nishihara, K. Kobayashi, T. Ono, J.-i. Ohe, Y. Tokura, T. Mineno, and J. Nitta, Nat. Commun. **3**, 1082 (2012).
[18] S.-T. Lo, C.-H. Chen, J.-C. Fan, L. W. Smith, G. L. Creeth, C.-W. Chang, M. Pepper, J. P. Griffiths, I. Farrer, H. E. Beere, G. A. C. Jones, D. A. Ritchie, and T.-M. Chen, Nat. Commun. **8**, 15997 (2017).
[19] M. I. D'yakonov and V. I. Perel', Phys. Lett. A **35**, 459 (1971).
[20] M. I. D'yakonov, B. P. Zakharchenya, V. I. Perel, S. I. Safarov and V. G. Fleisher, Soviet Physics Uspekhi **14**, 806 (1972).
[21] N. Nagaosa, J. Sinova, S. Onoda, A. H. MacDonald, and N. P. Ong, Rev. Mod. Phys. **82**, 1539 (2010).
[22] J. Sinova, S. O. Valenzuela, J. Wunderlich, C. H. Back, and T. Jungwirth, Rev. Mod. Phys. **87**, 1213 (2015).
[23] V. M. Edelstein, Solid State Commun. **73**, 233 (1990).
[24] S. Ganichev, E. Ivchenko, and V. Belkov, Nature (London) **417**, 153 (2002).
[25] Y. K. Kato, R. C. Myers, A. C. Gossard, and D. D. Awschalom, Nature (London) **427**, 50 (2004).
[26] When the term *exchange* is used in this paper, it is in the sense of literal exchange of species between two channels and not quantum mechanical exchange.
[27] L. Van Dam, On the utilization of oxygen and regulation of breathing in some aquatic animals, Ph.D. thesis, Drukkerij Volharding, 1938.
[28] E. H. Hazelhoff and H. H. Evenhuis, Nature (London) **169**, 77 (1952).
[29] G. M. Hughes and M. Morgan, Biological Reviews **48**, 419 (1973).
[30] K. J. Ullrich, K. Kramer, and J. W. Boylan, Prog. Cardiovasc. Dis. **3**, 395 (1961).
[31] M. Randall and B. Longtin, Ind. Eng. Chem. **31**, 1295 (1939).
[32] J. W. Mitchell and G. E. Myers, Biophys. J. **8**, 897 (1968).
[33] J. M. Schicks, E. Spangenberg, R. Giese, M. Luzi-Helbing, M. Priegnitz, K. U. Heeschen, B. Strauch, J. Schrötter, J. Kück, M. Töpfer *et al.*, in *Offshore Technology Conference*, One Petro, Houston, Texas, May 2019.
[34] Z. G. Yu and M. E. Flatté, Phys. Rev. B **66**, 235302 (2002).
[35] S. Kos, M. Hruska, S. A. Crooker, A. Saxena, and D. L. Smith, Comput. Sci. Eng. **9**, 46 (2007).
[36] M. Wu, J. Jiang, and M. Weng, Phys. Rep. **493**, 61 (2010).
[37] N. J. Harmon, T. A. Peterson, C. C. Geppert, S. J. Patel, C. J. Palmstrøm, P. A. Crowell, and M. E. Flatté, Phys. Rev. B **92**, 140201(R) (2015).
[38] L. O'Brien, D. Spivak, N. Krueger, T. A. Peterson, M. J. Erickson, B. Bolon, C. C. Geppert, C. Leighton, and P. A. Crowell, Phys. Rev. B **94**, 094431 (2016).
[39] F. Meier and B. P. Zachachrenya, *Optical Orientation: Modern Problems in Condensed Matter Science* (North-Holland, Amsterdam, 1984), Vol. 8.

[40] J. M. Kikkawa and D. D. Awschalom, Phys. Rev. Lett. **80**, 4313 (1998).
[41] M. Sharan and A. S. Popel, Math. Biosci. **91**, 17 (1988).
[42] J. M. Kikkawa, I. P. Smorchkova, N. Samarth, and D. D. Awschalom, Science **277**, 1284 (1997).
[43] Z. G. Yu and M. E. Flatté, Phys. Rev. B **66**, 201202(R) (2002).
[44] T. Tahara, Y. Ando, M. Kameno, H. Koike, K. Tanaka, S. Miwa, Y. Suzuki, T. Sasaki, T. Oikawa, and M. Shiraishi, Phys. Rev. B **93**, 214406 (2016).
[45] M. K. Chan, Q. O. Hu, J. Zhang, T. Kondo, C. J. Palmstrøm, and P. A. Crowell, Phys. Rev. B **80**, 161206(R) (2009).
[46] T. Akiho, J. Shan, H. X. Liu, K. I. Matsuda, M. Yamamoto, and T. Uemura, Phys. Rev. B **87**, 235205 (2013).
[47] Z. Lin, K. Kondo, M. Yamamoto, and T. Uemura, Jpn. J. Appl. Phys. **55**, 04EN03 (2016).
[48] Y. Ohno, R. Terauchi, T. Adachi, F. Matsukura, and H. Ohno, Phys. Rev. Lett. **83**, 4196 (1999).
[49] X. Lou, C. Adelmann, S. A. Crooker, E. S. Garlid, J. Zhang, K. S. M. Reddy, S. D. Flexner, C. J. Palmstrøm, and P. A. Crowell, Nat. Phys. **3**, 197 (2007).
[50] M. Furis, D. L. Smith, S. Kos, E. S. Garlid, K. S. M. Reddy, C. J. Palmstrøm, P. A. Crowell, and S. A. Crooker, New J. Phys. **9**, 347 (2007).
[51] K. Olejník, J. Wunderlich, A. C. Irvine, R. P. Campion, V. P. Amin, J. Sinova, and T. Jungwirth, Phys. Rev. Lett. **109**, 076601 (2012).
[52] A. Cohen, J. Phys. Chem. A **113**, 11084 (2009).
[53] M. Kustov, P. Laczkowski, D. Hykel, K. Hasselbach, F. Dumas-Bouchiat, D. OBrien, P. Kauffmann, R. Grechishkin, D. Givord, G. Reyne, O. Cugat, and N. M. Dempsey, J. Appl. Phys. **108**, 063914 (2010).
[54] V. Zablotskii, T. Polyakova, O. Lunov, and A. Dejneka, Sci. Rep. **6**, 37407 (2016).
[55] D. Paget, G. Lampel, B. Sapoval, and V. I. Safarov, Phys. Rev. B **15**, 5780 (1977).
[56] N. J. Harmon and M. E. Flatté, Phys. Rev. B **106**, 054207 (2022).
[57] C. Geppert, K. Christie, M. Chan, S. Patel, C. Palmstrøm, and P. Crowell, in *APS March Meeting Abstracts* (Baltimore, MD, 2013), Vol. 2013, pp. C18–010.